EES Catalysis

PAPER

View Article Online
View Journal | View Issue

Cite this: *EES Catal.*, 2024, 2, 1285

Medium entropy alloy wavy nanowires as highly effective and selective alcohol oxidation reaction catalysts for energy-saving hydrogen production and alcohol upgrade†

Xiaoyang Fu,[ad] Chengzhang Wan,[a] Huaixun Huyan,[c] Sibo Wang,[a] Ao Zhang,[b] Jingxuan Zhou,[b] Hongtu Zhang,[a] Xun Zhao,[e] Jun Chen,[e] Xiaoqing Pan,[c] Yu Huang *[b] and Xiangfeng Duan *[a]

Received 27th April 2024,
Accepted 24th July 2024

DOI: 10.1039/d4ey00090k

rsc.li/eescatalysis

Alcohol-assisted water electrolysis offers an attractive path for on-demand hydrogen generation while concurrently producing value added carboxylates. However, the anodic alcohol oxidation reaction (AOR) often requires precious metal-based catalysts, yet is still plagued with high overpotential or limited mass activity. Herein we report a facile synthesis of medium entropy Au-doped PtAgRhCu alloy wavy nanowires for highly efficient AORs. The alloy design facilitates hydroxyl adsorption that promotes the conversion of the carbonaceous intermediates (*e.g.* CH_3CO^*) to carboxylate products and weakens the adsorption of carboxylate products, resulting in greatly enhanced mass activity for four-electron AORs and highly selective upgrade of ethanol and ethylene glycol into value added acetate and glycolate. Furthermore, we constructed an alcohol assisted water electrolyser that delivers a current density of 100 mA cm^{-2} at a cell voltage lower than 0.6 V and a current density of 1 A cm^{-2} at a cell voltage of 1.2 V.

Broader context

Alcohol-assisted water electrolysis offers an energy-efficient method for hydrogen production by replacing the water oxidation reaction with the alcohol oxidation reaction (AOR), concurrently producing value-added carboxylate products. The primary challenge lies in developing electrocatalysts with high activity and selectivity. We present the design and synthesis of Au-doped PtAgRhCu alloy wavy nanowire electrocatalysts, demonstrating ultrahigh mass activity and selectivity for the 4-electron ethanol and ethylene glycol oxidation reactions. The enhanced activity and selectivity are attributed to facilitated hydroxyl adsorption, which promotes the conversion of carbonaceous intermediates, and weakened adsorption of carboxylate products. This leads to alcohol-assisted water electrolysis for energy-efficient hydrogen production while yielding value-added acetate or glycolate products, achieving nearly 100% faradaic efficiency and reducing the cell voltage by at least 0.2 V to reach 100 mA cm^{-2}, compared to previously reported state-of-the-art noble metal-based electrocatalysts. This study could inspire further advancements in energy-efficient hydrogen production along with selective alcohol upgrading.

Introduction

Alcohol-assisted water electrolysis offers an appealing path for on-demand green hydrogen production.[1] The alcohol oxidation reaction (AOR) features a greatly lower thermodynamic oxidation potential (<0.1 V *vs.* RHE)[1] than that of the water oxidation reaction (1.23 V *vs.* RHE) and could greatly reduce the required energy input for hydrogen production. At the same time, the AOR could produce value-added carboxylates products with additional economic value. Additionally, some alcohols, such as glycerol and ethylene glycol (EG), are also found in industrial waste and considered as environmental pollutants,[2,3] therefore, the oxidation of these alcohols could bring additional environmental benefits in terms of alcohol waste treatment.

However, the AOR is kinetically sluggish with a high overpotential and often requires costly noble metal-based electrocatalysts. Improving the mass activity (MA) and durability of such catalysts represents a central research target for the field.

[a] *Department of Chemistry and Biochemistry, University of California, Los Angeles, Los Angeles, CA 90095, USA. E-mail: xduan@chem.ucla.edu*
[b] *Department of Materials Science and Engineering, University of California, Los Angeles, Los Angeles, CA 90095, USA. E-mail: yhuang@seas.ucla.edu*
[c] *Department of Materials Science and Engineering, University of California, Irvine, Irvine, CA 92697, USA*
[d] *School of Materials Science and Engineering, Peking University, Beijing, 100871, China*
[e] *Department of Bioengineering, University of California, Los Angeles, Los Angeles, CA 90095, USA*

† Electronic supplementary information (ESI) available. See DOI: https://doi.org/10.1039/d4ey00090k

Alloying has been a very popular strategy in electrocatalyst design to enhance the specific activity (SA) for the AOR:[4,5] oxophilic metals (*e.g.* Ru,[6–8] Ni[9]) have been employed to facilitate the adsorption of surficial hydroxyl groups which is beneficial for dehydrogenation and CO removal steps during the AOR *via* the Langmuir–Hinshelwood (L–H) mechanism (bifunctional effect). Alloying with different metals may also produce a ligand effect and strain effect that can tune the electronic structure and d-band structure, and thus modulate the interactions with different reaction intermediates and adsorbates to enhance the performances.[10,11] Recently, high entropy and medium entropy alloy nanostructures have also attracted tremendous research interests as electrocatalysts.[12,13] In particular, the fluctuation of lattice potential energy due to the varied surrounding atoms increases the energy barrier for the atom migration, which could help improve the stability of the electrocatalysts (sluggish diffusion effect).[14,15] In addition, the multicomponent alloy could also bring in an additional synergistic effect (cocktail effect) to enhance the SA.[12,13]

Therefore, we proposed an Au-doped PtAgRhCu alloy system with medium mixing entropy (~1.45 R), which is close to the entropy level of the high entropy alloy (1.5 R) as defined by previous literature,[12,13,16] as a highly efficient AOR catalyst. Rh, due to its oxophilicity, can facilitate the hydroxyl group formation, which thus facilitates the dehydrogenation steps and conversion of carbonaceous intermediates during the AOR *via* the bifunctional effect.[17,18] Au is also reported to benefit the AOR since the higher atomic radius can induce tensile strain to facilitate the adsorption of alcohol and hydroxyl groups.[19] While Ag and Cu could be beneficial to weaken the binding with the carbonaceous intermediates and carboxylates products,[20,21] and their high conductivity is also beneficial for more efficient charge delivery for electrocatalysis.[22] In addition to the ligand effect, strain effect and bifunctional effect, the cocktail effect and sluggish diffusion effect could potentially further boost the SA and the durability of the resulting alloy catalysts.[14,15]

Ultrathin wavy nanowire is an attractive morphology for electrocatalysts as the ultrathin diameter can lead to a high specific surface area, thus contributing to a high electrochemical active surface area (ECSA),[22] an equally important factor to improve MA; the surface defects on the wavy nanowires can contribute to catalytic sites for further enhanced performances;[23,24] while the one-dimensional nanostructure is beneficial for efficient charge transport to and from the catalytic active sites to ensure efficient utilization of the active sites in electrocatalysis.[24,25]

Herein, we reported a facile synthesis of medium entropy Au-doped PtAgRhCu alloy wavy nanowires as highly effective electrocatalysts for the ethanol oxidation reaction (EOR) and ethylene glycol oxidation reaction (EGOR). The resulting nanowires feature an ultrafine diameter of 3.7 ± 1.0 nm, deliver an ultrahigh MA of 8.43 ± 0.40 A $mg_{noble\ metal}^{-1}$ for the EOR and 23.2 ± 1.4 A $mg_{noble\ metal}^{-1}$ for the EGOR, respectively, and exhibit good long-term performance in chronoamperometry (CA) tests. The resulting nanowires show robust performance for alcohol assisted water electrolysis, achieving a current density of 100 mA cm^{-2} at a cell voltage of <0.6 V, about ~1 V lower than that of conventional water electrolysis. More importantly, apart from energy-efficient hydrogen production, the system produces value-added products, such as acetates and glycolates from EtOH and EG with nearly 100% faradaic efficiency (FE).

Results and discussion

Characterization

A transmission electron microscopy (TEM) study reveals the wavy nanowire morphology (Fig. 1a) with the diameters mostly ranging between 2.0 and 5.5 nm and an average diameter of 3.7 ± 1.0 nm (Fig. 1b), which could promise a high specific surface area and high ECSA. The wavy nanowire morphology with surface steps may contribute the catalytic sites. X-ray diffraction (XRD) also demonstrates a single phase face-centered cubic (FCC) crystal lattice structure with the peaks corresponding to the (111), (200), (220) and (311) crystal planes (Fig. 1c) positioned amid those corresponding peaks of the FCC Pt (JCPDS no. 04-0802), Ag (JCPDS no. 04-0783), Rh (JCPDS no. 05-0685), Cu (JCPDS no. 04-0836) and Au (JCPDS no. 01-1172) without any other distinct phases, indicating the formation of a uniform alloy phase. Based on the peak width, an average crystallite size of 2.2 nm was approximately estimated from the Scherrer's equation. Energy dispersive X-ray spectroscopy (EDX) mapping images and linescans for all five elements further demonstrate the uniform distribution of the Pt, Ag, Rh, Cu and Au in the nanowire structure with a ratio of 21.7% : 23.5% : 26.9% : 21.9% : 6.0%, confirming the formation of the medium entropy Au-doped PtAgRhCu alloy (Fig. 1d and Fig. S1, ESI†) despite minor Au segregation. Inductively coupled plasma atomic emission spectroscopy (ICP-AES) reveals an elemental composition of Pt : Ag : Rh : Cu : Au = 1.00 : 1.09 : 0.97 : 0.71 : 0.085, which generally agrees with the feed ratio of the precursors. The content of Cu is lower than the feed ratio, which could be attributed to the lower redox potential of Cu^{2+}/Cu compared with the noble metal counterparts and thus is more difficult to be reduced during the synthesis. X-ray photoelectron spectroscopy (XPS) also demonstrates the presence of Pt, Ag, Rh, Cu, and Au elements with peaks at 70.9 eV (Pt $4f_{7/2}$), 367.7 eV (Ag $3d_{5/2}$), 307.0 eV (Rh $3d_{5/2}$), 932.0 eV (Cu $2p_{3/2}$) and 83.8 eV (Au $4f_{7/2}$), respectively (Fig. S2, ESI†). The binding energies of Pt $4f_{7/2}$ (shifted from ~71.3 eV for commercial Pt/carbon black[26] to 70.9 eV), Rh $3d_{5/2}$ (shifted from ~307.35 eV for Rh wavy nanowire[23,24] to 307.0 eV) and Au $4f_{7/2}$ (shifted from ~84.5 eV for Au nanowire[27] to 83.8 eV) are negatively shifted while the binding energies of Ag $3d_{5/2}$ (from 367.35 eV for Ag nanowire[28] to 367.7 eV) and Cu $2p_{3/2}$ (from 931.8 eV for Cu nanowire[29] to 932.0 eV) are positively shifted, indicating the electron transfer from Ag and Cu to Pt, Rh and Au (in agreement with their difference in electronegativity (Pt: 2.28, Rh: 2.28, Au: 2.54, Ag: 1.93, Cu: 1.90)), which could modify the electronic structure and benefit the AOR performance by weakening the binding of the carbonaceous species, such as the CH_3CO^* intermediate during the EOR[30] and $HOCH_2CO^*$ intermediate during the EGOR,[31] leading to enhanced EOR and EGOR performance. For comparison, the PtAgRh and PtAgRhCu alloy wavy

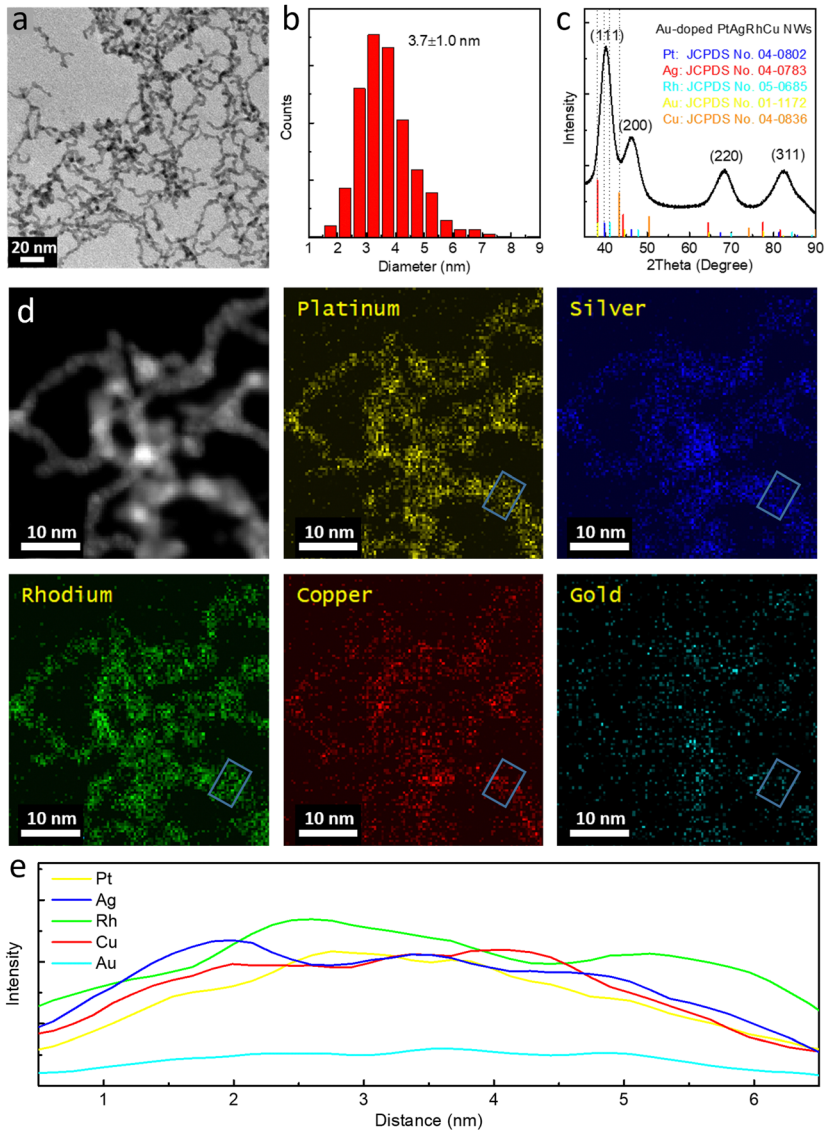

Fig. 1 Characterizations. (a) TEM pictures of medium entropy Au-doped PtAgRhCu alloy wavy nanowires. (b) The diameter distribution of medium entropy Au-doped PtAgRhCu alloy wavy nanowires. (c) XRD pattern of medium entropy Au-doped PtAgRhCu alloy wavy nanowires. (d) STEM and EDX mapping of medium entropy Au-doped PtAgRhCu alloy wavy nanowires (L-edge signals for all elements). (e) Linescan results (blue region).

nanowires were also synthesized with similar nanowire morphology (Fig. S3, ESI†). The binding energies in Au-doped PtAgRhCu are rather similar to those in PtAgRhCu nanowires, with less than 0.05 eV difference (Fig. S4, ESI†), which could be attributed to the limited impact on binding energy shift due to the low content of Au doping. In addition, when comparing the PtAgRhCu nanowires with PtAgRh nanowires (Fig. S4 and S5, ESI†), the binding energies of Pt and Rh are $\sim$0.1 eV lower, which also agrees with the charge transfer from Cu.

Electrochemical study

The ECSAs of the wavy nanowires were determined from the hydrogen underpotential deposition (HUPD) measurement in 0.1 M $HClO_4$ (Fig. S6, ESI†) with a similar ECSA value ($\sim$40 m^2 g^{-1}) due to similar morphologies. The commercial Pt/graphitic carbon (Pt/GC) have a higher ECSA value of 50.2 $\pm$ 1.2 m^2 g^{-1}.

The EOR performance was studied in 1.0 M KOH + 1.0 M EtOH *via* cyclic voltammetry (CV) at a scan rate of 50 mV s^{-1} (Fig. 2a). The medium entropy Au-doped PtAgRhCu alloy wavy nanowires demonstrate the best EOR performances with an ultrahigh MA of 8.43 $\pm$ 0.40 A $mg_{noble\ metal}^{-1}$ and SA of 22.1 $\pm$ 2.3 mA cm^{-2}, which is much higher than those of the PtAgRh nanowire and PtAgRhCu nanowires. According to the current understanding of the 4-electron oxidation mechanism of the EOR, the adsorbed EtOH undergoes dehydrogenation steps initially, leading to the CH_3CHO^*/CH_3CO^* intermediate, which then reacts with $-OH_{ad}$ on the nearby sites to produce acetate.[4] Rh, as a highly oxophilic component, could facilitate the adsorption of $-OH_{ad}$ and promote the further conversion of CH_3CHO^*/CH_3CO^* intermediate to acetate, thus enhancing the EOR performance as shown in the previous report of PtRh alloy.[18] The introduction of Ag and Cu has been reported to

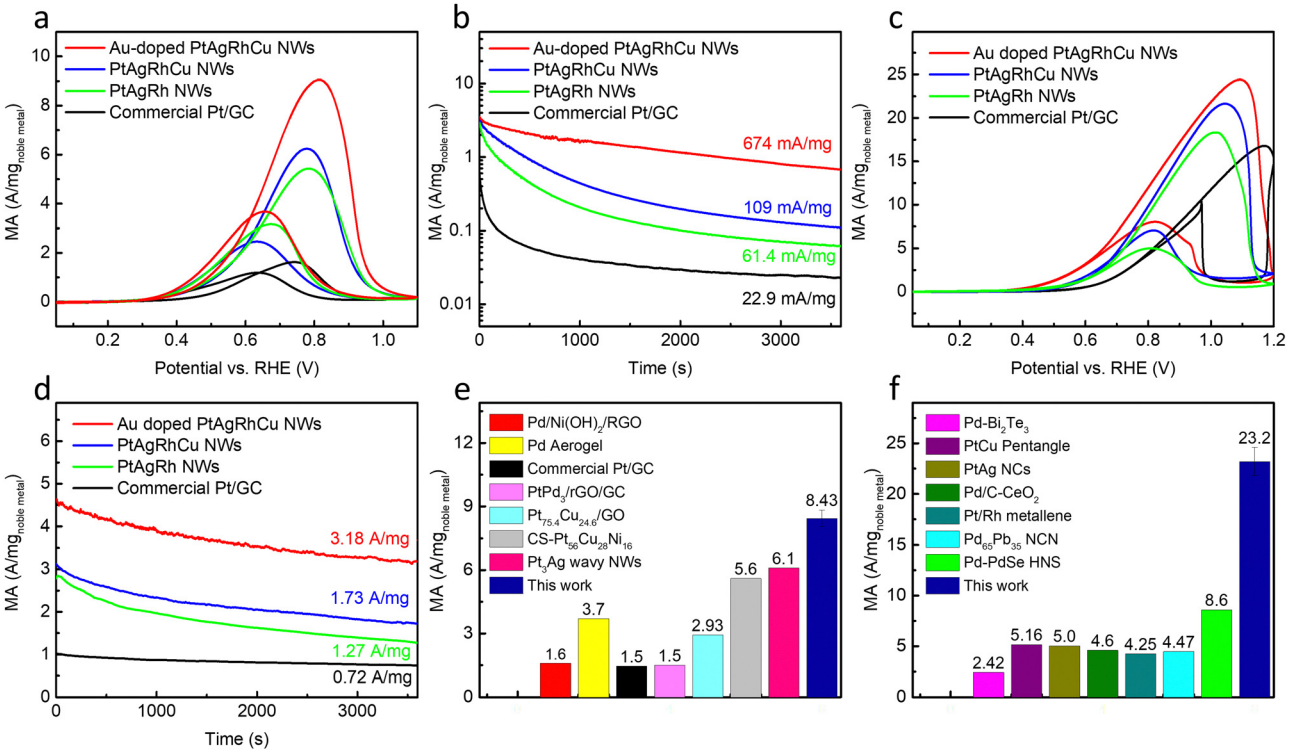

Fig. 2 Electrocatalytic study of the electrocatalysts. (a) Mass-normalized CV curves of the electrocatalysts in 1.0 M KOH + 1.0 M EtOH electrolyte at a scan rate of 50 mV s^{-1}. (b) CA results of the electrocatalysts in 1.0 M KOH + 1.0 M EtOH electrolyte at 0.67 V *vs.* RHE. (c) Mass-normalized CV curves of the electrocatalysts in 1.0 M KOH + 1.0 M EG electrolyte at a scan rate of 50 mV s^{-1}. (d) CA results of the electrocatalysts in 1.0 M KOH + 1.0 M EG electrolyte at 0.67 V *vs.* RHE. (e) Summary and comparison of the EOR performances with previously reported electrocatalysts. (f) Summary and comparison of the EGOR performances with previously reported electrocatalysts.

boost the EOR performance,[30,32,33] by adjusting the d-band structure and weakening the adsorption of CH_3CHO^*/CH_3CO^* intermediates, which lowers the reaction barrier to the acetate as suggested by DFT calculation.[30] In addition, Ag and Cu has also been widely reported as electrocatalysts for CO_2 or CO reduction reaction to acetate, consistent with their capability to facilitate the desorption of acetate as well.[20,21,34] Furthermore, Au has been reported to induce tensile strain due to its higher atomic radius and could thus facilitate the adsorption of ethanol and $-OH_{ad}$,[19,35] which is beneficial to the 4-electron oxidation pathway for the EOR. Lastly, there may also be some additional synergy (so called "cocktail effect") from alloys with higher entropy that is yet to be fully understood. Compared with the commercial Pt/GC (MA of 1.46 ± 0.12 A mg^{-1} and SA of 2.88 ± 0.27 mA cm^{-2}), the MA and SA of the Au-doped PtAgRhCu alloy wavy nanowires showed nearly 6-time and 8-time improvements, respectively.

CA tests were conducted to study the long-term performances of the electrocatalysts (Fig. 2b). Significantly, the medium entropy Au-doped PtAgRhCu alloy wavy nanowires demonstrate considerably better long-term performances, maintaining a current of 674 mA mg^{-1} after 1 h at 0.67 V *vs.* RHE, which is nearly 30 times higher than that of the commercial Pt/GC under the same conditions (only 22.9 mA mg^{-1}). Apart from the previously discussed facilitated hydroxyl group adsorption to promote the dehydrogenation and conversion of the carbonaceous intermediates as well as the facilitated desorption of the carboxylate products, this improvement may also be partially attributed to the sluggish diffusion effect that stabilizes the medium/high-entropy alloy by inhibiting the atom diffusions.[14,15]

We have further explored the EGOR performance of the Au-doped PtAgRhCu alloy wavy nanowires in 1.0 M KOH + 1.0 M EG electrolyte, revealing an ultrahigh MA of 23.2 ± 1.4 A $mg_{noble\ metal}^{-1}$ (Fig. 2c). Compared with PtAgRh nanowire, PtAgRhCu nanowires and commercial Pt/GC, the MA in the lower potential region receives more evident enhancement. For example, the MA at 0.67 V shows a 4-fold enhancement over the commercial Pt/GC. The CA tests also demonstrate outstanding current retention of 3.18 A $mg_{noble\ metal}^{-1}$ after a 1 h test (Fig. 2d), and this performance can be generally recovered *via* a few CV scans, leading to sustained long-term performance with a retained current of 2.88 A $mg_{noble\ metal}^{-1}$ for a cumulative of 9 h CA testing (Fig. S7, ESI†). Considering the EGOR also proceeds in the 4-electron pathway with glycolate as the final product *via* a similar mechanism that starts with the EG adsorption, followed by the dehydrogenation and the intermediate ($HOCH_2CO^*$) conversion to glycolates,[31] our aforementioned electrocatalyst design is also beneficial, with Rh promoting $-OH_{ad}$ formation to facilitate the intermediate conversion, Ag and Cu weakening the adsorption of $HOCH_2CO^*$ intermediate and glycolate product, and Au facilitating the –OH

Table 1 Comparison with the previous literature in terms of the long-term performances of the AOR in alkaline media

Materials	Electrolyte	Current maintained [A mg^{-1}]	Potential *vs.* /it> *RHE [V]*	Time [h]	Ref.
Au-doped PtAgRhCu alloy wavy nanowire	1.0 M KOH + 1.0 M EtOH	0.67	0.67	1.0	This work
Au-doped PtAgRhCu alloy wavy nanowire	1.0 M KOH + 1.0 M EG	3.18	0.67	1.0	This work
Commercial Pt/GC	1.0 M KOH + 1.0 M EtOH	0.02	0.67	1.0	This work
Commercial Pt/GC	1.0 M KOH + 1.0 M EG	0.72	0.67	1.0	This work
Core–shell $Pt_{56}Cu_{28}Ni_{16}$ tetrahedra	1.0 M KOH + 1.0 M EtOH	~0.1	0.65	1.0	40
Pt_3Ag wavy NWs	1.0 M KOH + 1.0 M EtOH	0.15	0.72	1.7	26
Pd/$Ni(OH)_2$/rGO	1.0 M KOH + 1.0 M EtOH	0.44	0.86	5.6	36
Core@shell Au@PtIr	1.0 M KOH + 1.0 M EtOH	0.28	0.45	1.7	19
Core@skin PtBi@Pt	1.0 M KOH + 1.0 M EtOH	0.48	0.62	0.5	42
$PtPd_3$/rGO/GC	1.0 M KOH + 1.0 M EtOH	0.08	0.71	1.0	38
Pd–Bi_2Te_3	1.0 M KOH + 1.0 M EG	0.62	0.82	1.0	43
PtCu pentangle	1.0 M KOH + 1.0 M EG	0.44	0.87	1.0	44
PtAg NCs	1.0 M KOH + 1.0 M EG	0.1	1.05	1.0	45
Pd/C–CeO_2	1.0 M KOH + 1.0 M EG	0.14	0.72	1.0	46
Pt/Rh metallene	1.0 M KOH + 3.0 M EG	0.7	N/A	1.0	47
$Pd_{65}Pb_{35}$ NCN	1.0 M KOH + 1.0 M EG	0.55	0.72	1.0	48
Pd–PdSe HNS	1.0 M KOH + 1.0 M EG	1.1	0.7	1.0	49

and EG adsorption, which ultimately leads to enhanced EGOR performance.

Compared with many previously reported highly effective electrocatalysts, such as Pd/$Ni(OH)_2$/rGO,[36] Pd Aerogel,[37] $PtPd_3$/rGO/GC,[38] $Pt_{75.4}Cu_{24.6}$/GO,[39] core–shell (CS) $Pt_{56}Cu_{28}Ni_{16}$ tetrahedra,[40] single atom Ni–Pt (SANi-Pt) NWs,[41] and Pt_3Ag wavy NWs,[26] the Au-doped PtAgRhCu alloy wavy nanowires showed much improved MA (Fig. 2e). Notably, our electrocatalysts also greatly outperform the previously reported state-of-the-art noble metal based electrocatalysts[36–41] for the EGOR with at least 3-fold higher MA (Fig. 2f). Furthermore, the Au-doped PtAgRhCu electrocatalysts also demonstrate great stability for the EOR and EGOR from CA tests with a retained current of 674 mA mg^{-1} and 3.18 A mg^{-1} after 1 h test, respectively, which far outperforms the CA performance reported in previous literature as shown in Table 1.

Alcohol assisted water electrolysis

Moving a step further, we constructed a membrane electrode assembly (MEA)[50] and tested the performance of our electrocatalysts in alcohol assisted water electrolysis. With Au-doped PtAgRhCu alloy wavy nanowires as the anode electrocatalysts and commercial Pt/GC as the cathode HER electrocatalysts, the resulting MEA delivers a high level of current density of 100 mA cm^{-2} at a voltage of 0.49 V and an ultrahigh geometric current density of 1.0 A cm^{-2} at 1.2 V for the EtOH assisted water electrolysis (Fig. 3a). The performance and robustness significantly outperform the electrolyser employing commercial Pt/GC as both the cathode and anode that showed much lower geometric current density (<200 mA cm^{-2}) and extremely rapid performance decay due to the much poorer stability of commercial Pt/GC in the EOR (Fig. 3b). In the case of EG assisted water electrolyser, our electrocatalysts also demonstrate excellent performance (cell voltages of 0.57 V at 100 mA cm^{-2} in Fig. 3c) as well as robustness, with less than 50 mV voltage increase after 10 h CP test at 100 mA cm^{-2} (Fig. 3d).

Notably, the performance can be generally recovered upon refreshing electrolytes after each CP test (Fig. S8, ESI†) and the polarization curve can be recovered as well (Fig. S9, ESI†). Compared with a traditional water electrolyser, an alcohol-assisted water electrolyser can evidently lower the required voltage, for example, 1.06 V was lowered in the EtOH-assisted water electrolyser compared with the counterpart without EtOH (Fig. 3e). Remarkably, our electrocatalysts, when combined with the MEA process, only requires 0.49 V and 0.57 V, respectively for the EtOH and EG assisted water electrolyser to achieve a high current density of 100 mA cm^{-2}, which is at least 0.2 V lower than those with the previously reported noble metal based electrocatalysts, such as Pt holey nanotubes (hNTs),[51] RhFeNi phosphide nanosheets (NSs),[52] Ru/$Ni(OH)_2$[53] for EtOH assisted water electrolysis, Pd/TiO_2,[54] Pt–Ir metallene,[55] Ru/Ni_2P/NF[56] and Au/$Ni(OH)_2$[57] for EG assisted water electrolysis (Fig. 3f). Further analyses of the oxidation product reveal highly selective EOR and EGOR, with acetate as the predominant EOR product with FE of 99.8 ± 1.0%, and glycolate was the predominant EGOR product with FE of 100.7 ± 1.8% (Fig. S10, ESI†). The production rates of acetate and glycolate as 4-electron oxidation products are 0.931 ± 0.009 mmol h^{-1} and 0.939 ± 0.017 mmol h^{-1}, respectively. In addition, the aliquot after EGOR was also tested with Ca^{2+} and excessive acetic acid and no precipitation were observed, which further confirms the absence of oxalate byproduct.

We have further evaluated the anode electrocatalysts after the EOR and EGOR CP tests. TEM studies indicate the wavy nanowire morphology is well retained (Fig. S11, ESI†). The XRD pattern also demonstrates the maintained crystal structure (Fig. S12, ESI†). XPS demonstrates the generally unchanged binding energies and oxidation states for Pt, Ag, Rh and Au elements, while the greatly lowered Cu oxide peak content could be attributed to the removal of surficial Cu oxide species during the activation process in acidic media (Fig. S13 and S14, ESI†). During the CP test, negligible dissolution of Pt, Ag, Rh, Cu and Au ($\ll 0.1\%$) was confirmed from the inductively coupled plasma-mass spectrometry (ICP-MS) measurements, confirming the stability of our electrocatalysts under a long-term test period.

From a technoeconomic perspective, the lowered voltage requirement (~1 V) could save 26.8 kW h electrical energy for

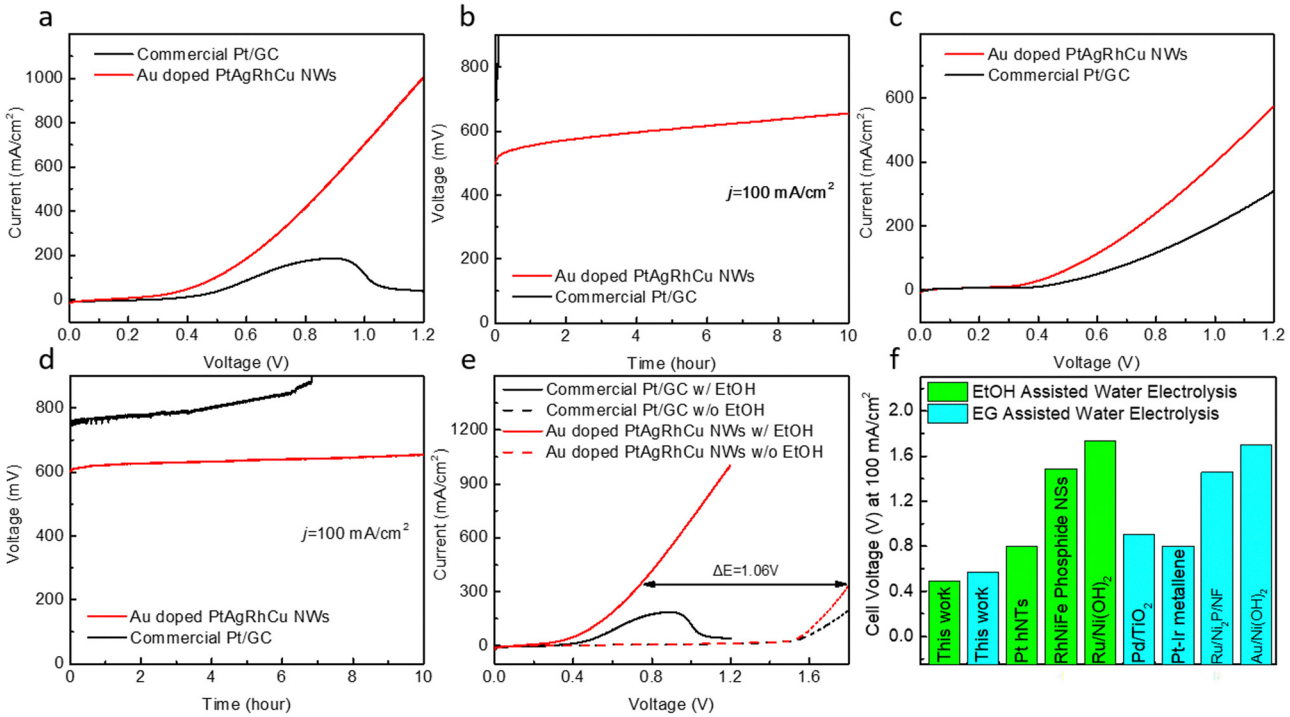

Fig. 3 Alcohol assisted water electrolysis. (a) Polarization curves of the electrolysers in the 1.0 M KOH + 1.0 M EtOH electrolyte. (b) CP tests of the electrolysers at a current density of 100 mA cm^{-2} in the 1.0 M KOH + 1.0 M EtOH electrolyte. (c) Polarization curves of the electrolysers in the 1.0 M KOH + 1.0 M EG electrolyte. (d) CP tests of the electrolysers at a current density of 100 mA cm^{-2} in the 1.0 M KOH + 1.0 M EG electrolyte. (e) Comparison of the polarization curves in 1.0 M KOH + 1.0 M EtOH electrolyte and 1.0 M KOH electrolyte. (f) Performance comparison with the previously reported state-of-the-art noble-metal-based alcohol assisted water electrolysers.

1 kg H_2 production, which is equivalent to \$4.07 per kgH_2 considering the industrial electricity cost of \$0.152 per kW h in California. More importantly, this process also leads to value added carboxylates products. In the US market, the commodity price of potassium acetate is 1.24 k\$ per ton, equivalent to a molar price of 0.122 \$ per mol, which is more than 4-fold higher compared with EtOH (0.591 k\$ per ton, 0.027 \$ per mol) when considering the scenario of molar conversion. More significantly, glycolic acid with a rapidly growing market size, has a molar price (3.20 k\$ per ton, 0.243 \$ per mol) more than 8-fold higher than EG (0.468 k\$ per ton, 0.029 \$ per mol), offering a highly attractive and promising economic prospect. Another important aspect is that EG is also commonly produced as a petrochemical industrial waste and can cause environmental issues so that the electrooxidation of them may also bring significant environmental benefits.[3]

Conclusions

In conclusion, we have reported a straightforward solvothermal synthesis of ultrafine medium entropy Au-doped PtAgRhCu alloy wavy nanowires as highly active and selective EOR and EGOR catalysts. The greatly boosted alcohol oxidation performance and robustness can be attributed to a combination of ligand effect, strain effect, and bifunctional effect to facilitate the hydroxyl adsorption, promote dehydrogenation and conversion of carbonaceous intermediates, and facilitate carboxylate desorption during the AORs, in addition to the cocktail effect and sluggish diffusion effect in alloy catalysts. Our studies demonstrated outstanding performance and robustness for alcohol assisted water electrolysis, achieving a current density of 100 mA cm^{-2} at a cell voltage <0.6 V, which is at least 0.2 V lower compared with the state-of-the-art in previous reports. Product analysis confirm highly selective oxidation of alcohol and ethylene glycol to produce value-added chemicals such as acetate and glycolate with nearly 100% FE. We expect this study could inspire more efforts in the field of energy-saving hydrogen production and selective alcohol upgrading.

Author contributions

X. F., Y. H. and X. D. conceived and designed this research. X. F. synthesized the electrocatalysts and studied the electrocatalytic performance. X. F., C. W., H. H., S. W., A. Z., J. Z., H. Z. and X. P. contributed to the characterization. X. F. carried out the alcohol assisted water electrolysis test with assistance from X. Z. and J. C. All authors contributed to the analysis and interpretation of the results. X. F., Y. H. and X. D. wrote the manuscript.

Data availability

The data supporting this article have been included as part of the ESI.†

Conflicts of interest

There are no conflicts to declare.

Acknowledgements

X. D. and Y. H. acknowledge the generous support from New-Hydrogen, Inc. X. F. acknowledges the generous support from the Red Avenue Development Fund.

References

1 H. Wang, M. Sun, J. Ren and Z. Yuan, *Adv. Energy Mater.*, 2023, **13**, 2203568.
2 J. Kou, C. Bennett-Stamper and R. S. Varma, *ACS Sustainable Chem. Eng.*, 2013, **1**, 810–816.
3 A. Elreedy, E. Ibrahim, N. Hassan, A. El-Dissouky, M. Fujii, C. Yoshimura and A. Tawfik, *Energy Convers. Manag.*, 2017, **140**, 133–144.
4 J. Bai, D. Liu, J. Yang and Y. Chen, *ChemSusChem*, 2019, **12**, 2117–2132.
5 X. Fu, C. Wan, Y. Huang and X. Duan, *Adv. Funct. Mater.*, 2022, **32**, 2106401.
6 S. Zhao, H. Yin, L. Du, G. Yin, Z. Tang and S. Liu, *J. Mater. Chem. A*, 2014, **2**, 3719–3724.
7 S. Lu, K. Eid, D. Ge, J. Guo, L. Wang, H. Wang and H. Gu, *Nanoscale*, 2017, **9**, 1033–1039.
8 C. Xu, L. Wang, X. Mu and Y. Ding, *Langmuir*, 2010, **26**, 7437–7443.
9 Q. Jiang, L. Jiang, S. Wang, J. Qi and G. Sun, *Catal. Commun.*, 2010, **12**, 67–70.
10 B. Hammer and J. K. Norskov, in *Advances in Catalysis, Vol 45 Impact of Surface Science on Catalysis*, ed. B. C. Gates and H. Knozinger, Elsevier Academic Press Inc, San Diego, 2000, vol. 45, pp. 71–129.
11 M. Mavrikakis, B. Hammer and J. K. Norskov, *Phys. Rev. Lett.*, 1998, **81**, 2819–2822.
12 X. Wang, W. Guo and Y. Fu, *J. Mater. Chem. A*, 2021, **9**, 663–701.
13 Y. Xin, S. Li, Y. Qian, W. Zhu, H. Yuan, P. Jiang, R. Guo and L. Wang, *ACS Catal.*, 2020, **10**, 11280–11306.
14 Y. Wang, W. Luo, S. Gong, L. Luo, Y. Li, Y. Zhao and Z. Li, *Adv. Mater.*, 2023, **35**, 2302499.
15 Y. Zhang, D. Wang and S. Wang, *Small*, 2022, **18**, 2104339.
16 J. W. Yeh, *JOM*, 2013, **65**, 1759–1771.
17 S. Shen, T. Zhao and J. Xu, *Int. J. Hydrogen Energy*, 2010, **35**, 12911–12917.
18 T. F. M. Moreira, S. A. Neto, C. Lemoine, K. B. Kokoh, C. Morais, T. W. Napporn and P. Olivi, *RSC Adv.*, 2020, **10**, 35310–35317.
19 Z. Liang, L. Song, S. Deng, Y. Zhu, E. Stavitski, R. R. Adzic, J. Chen and J. Wang, *J. Am. Chem. Soc.*, 2019, **141**, 9629–9636.
20 E. Landaeta, N. I. Kadosh and Z. D. Schultz, *ACS Catal.*, 2023, **13**, 1638–1648.
21 X. Yang, E. A. Fugate, Y. Mueanngern and L. R. Baker, *ACS Catal.*, 2017, **7**, 177–180.
22 X. Zhao, H. Zhang, Y. Yan, J. Cao, X. Li, S. Zhou, Z. Peng and J. Zeng, *Angew. Chem., Int. Ed.*, 2017, **56**, 328–332.
23 X. Huang, Z. Zhao, Y. Chen, C.-Y. Chiu, L. Ruan, Y. Liu, M. Li, X. Duan and Y. Huang, *Nano Lett.*, 2014, **14**, 3887–3894.
24 X. Fu, Z. Zhao, C. Wan, Y. Wang, Z. Fan, F. Song, B. Cao, M. Li, W. Xue, Y. Huang and X. Duan, *Nano Res.*, 2019, **12**, 211–215.
25 X. Fu, D. Cheng, C. Wan, S. Kumari, H. Zhang, A. Zhang, H. Huyan, J. Zhou, H. Ren, S. Wang, Z. Zhao, X. Zhao, J. Chen, X. Pan, P. Sautet, Y. Huang and X. Duan, *Adv. Mater.*, 2023, **35**, 2301533.
26 X. Fu, C. Wan, A. Zhang, Z. Zhao, H. Huyan, X. Pan, S. Du, X. Duan and Y. Huang, *Nano Res.*, 2020, **13**, 1472–1478.
27 X. Jiang, X. Qiu, G. Fu, J. Sun, Z. Huang, D. Sun, L. Xu, J. Zhou and Y. Tang, *J. Mater. Chem. A*, 2018, **6**, 17682–17687.
28 H. Mao, J. Feng, X. Ma, C. Wu and X. Zhao, *J. Nanopart. Res.*, 2012, **14**, 15.
29 I. F. Díaz Izaquita, L. Ortiz Espinel, N. Santos Santos, R. Cabanzo-Hernández and E. Mejía-Ospino, *MRS Adv.*, 2022, **7**, 981–986.
30 M. Pang, M. Yang, J. Yan, B. Zhang, L. Zang, A. Fu and P. Guo, *Langmuir*, 2022, **38**, 4287–4294.
31 F. Liu, X. Gao, R. Shi, Z. Guo, E. C. Tse and Y. Chen, *Angew. Chem., Int. Ed.*, 2023, **62**, e202300094.
32 H. Fu, N. Zhang, F. Lai, L. Zhang, S. Chen, H. Li, K. Jiang, T. Zhu, F. Xu and T. Liu, *ACS Catal.*, 2022, **12**, 11402–11411.
33 J. Huang, Q. Liu, Y. Yan, N. Qian, X. Wu, L. Ji, X. Li, J. Li, D. Yang and H. Zhang, *Nanoscale Adv.*, 2022, **4**, 111–116.
34 X. Q. Duan, G. Y. Duan, Y. F. Wang, X. Q. Li, R. Wang, R. Zhang and B. H. Xu, *Small*, 2023, **19**, 2207219.
35 K. Wei, H. Lin, X. Zhao, Z. Zhao, N. Marinkovic, M. Morales, Z. Huang, L. Perlmutter, H. Guan and C. Harris, *J. Am. Chem. Soc.*, 2023, **145**, 19076–19085.
36 W. Huang, X. Y. Ma, H. Wang, R. Feng, J. Zhou, P. N. Duchesne, P. Zhang, F. Chen, N. Han, F. Zhao, J. Zhou, W. B. Cai and Y. Li, *Adv. Mater.*, 2017, **29**, 1703057.
37 M. Z. Yazdan-Abad, M. Noroozifar, A. R. M. Alam and H. Saravani, *J. Mater. Chem. A*, 2017, **5**, 10244–10249.
38 F. Ren, H. Wang, C. Zhai, M. Zhu, R. Yue, Y. Du, P. Yang, J. Xu and W. Lu, *ACS Appl. Mater. Interfaces*, 2014, **6**, 3607–3614.
39 T. Liu, C. Li and Q. Yuan, *ACS Omega*, 2018, **3**, 8724–8732.
40 J. Huang, Y. Liu, M. Xu, C. Wan, H. Liu, M. Li, Z. Huang, X. Duan, X. Pan and Y. Huang, *Nano Lett.*, 2019, **19**, 5431–5436.
41 M. Li, K. Duanmu, C. Wan, T. Cheng, L. Zhang, S. Dai, W. Chen, Z. Zhao, P. Li, H. Fei, Y. Zhu, R. Yu, J. Luo, K. Zang, Z. Lin, M. Ding, J. Huang, H. Sun, J. Guo, X. Pan, W. A. Goddard, P. Sautet, Y. Huang and X. Duan, *Nat. Catal.*, 2019, **2**, 495–503.
42 B.-W. Zhang, W.-H. Lai, T. Sheng, X.-M. Qu, Y.-X. Wang, L. Ren, L. Zhang, Y. Du, Y.-X. Jiang and S.-G. Sun, *J. Mater. Chem. A*, 2019, **7**, 5214–5220.
43 H. Xu, B. Huang, Y. Zhao, G. He and H. Chen, *Inorg. Chem.*, 2022, **61**, 4533–4540.

44 H. Xu, C. Liu, P. Song, J. Wang, F. Gao, Y. Zhang, Y. Shiraishi, J. Di and Y. Du, *Chem. – Asian J.*, 2018, **13**, 626–630.
45 F. Gao, H. Xu, Y. Zhang, J. Wang, C. Wang and Y. Du, *Int. J. Hydrogen Energy*, 2018, **43**, 9644–9651.
46 S. Sankar, N. Watanabe, G. M. Anilkumar, B. N. Nair, S. G. Sivakamiammal, T. Tamaki and T. Yamaguchi, *Catal. Sci. Technol.*, 2019, **9**, 493–501.
47 H. Wang, Y. Liang, S. Liu, H. Yu, K. Deng, Y. Xu, X. Li, Z. Wang and L. Wang, *Inorg. Chem.*, 2023, **62**, 14477–14483.
48 B. Zou, Y. Zhang, F. Gao, Z. Li, C. Wang, Z. Wu, D. Wang and Y. Du, *Int. J. Hydrogen Energy*, 2022, **47**, 33329–33337.
49 Y. Qin, W. Zhang, F. Wang, J. Li, J. Ye, X. Sheng, C. Li, X. Liang, P. Liu and X. Wang, *Angew. Chem., Int. Ed.*, 2022, **61**, e202200899.
50 X. Fu, D. Cheng, A. Zhang, J. Zhou, S. Wang, X. Zhao, J. Chen, P. Sautet, Y. Huang and X. Duan, *Energy Environ. Sci.*, 2024, **17**, 2279–2286.
51 T.-J. Wang, H.-Y. Sun, Q. Xue, M.-J. Zhong, F.-M. Li, X. Tian, P. Chen, S.-B. Yin and Y. Chen, *Sci. Bull.*, 2021, **66**, 2079–2089.
52 J. Miao, X. Zhao, H.-Y. Hu, H. Huang, Y. Ding, Z.-H. Liu and Y. Chen, *ACS Appl. Nano Mater.*, 2022, **5**, 4948–4957.
53 W. Ao, C. Cheng, H. Ren, Z. Fan, P. Yin, Q. Qin, Z.-N. Chen and L. Dai, *ACS Appl. Mater. Interfaces*, 2022, **14**, 45042–45050.
54 Y. Chen, A. Lavacchi, H. Miller, M. Bevilacqua, J. Filippi, M. Innocenti, A. Marchionni, W. Oberhauser, L. Wang and F. Vizza, *Nat. Commun.*, 2014, **5**, 4036.
55 K. Deng, Z. Lian, W. Wang, J. Yu, H. Yu, Z. Wang, Y. Xu, L. Wang and H. Wang, *Small*, 2024, **20**, 2305000.
56 G. Ma, N. Yang, Y. Xue, G. Zhou and X. Wang, *ACS Appl. Mater. Interfaces*, 2021, **13**, 42763–42772.
57 Y. Yan, H. Zhou, S.-M. Xu, J. Yang, P. Hao, X. Cai, Y. Ren, M. Xu, X. Kong and M. Shao, *J. Am. Chem. Soc.*, 2023, **145**, 6144–6155.